B,V Observations and Analyses of the EW Stars NY Boötis and V508 Cygni

Andreas Beck
Schickhardtstraße 59, 71116 Gärtringen, Germany; Andreas.Beck@HFT-Stuttgart.de

Laurent Corp
56 Avenue de Paris, 12000 Rodez, France; astro.laucorp@orange.fr

Gerard Samolyk
P.O. Box 20677, Greenfield, WI 53220; gsamolyk@wi.rr.com

Received March 4, 2021; revised August 6, 2021, February 23, June 27, 2022; accepted July 2, 2022

Abstract This paper describes the acquisition of CCD-derived photometric data from two eclipsing overcontact binaries, NY Boo and V508 Cyg. Astrophotography filters (blue and green) were used, but measurements were transformed to the Johnson-Cousins standard using the reference star fields in M67. Aside from producing period-folded light curves for both variable systems, new times-of-minimum were added to other literature values in order to update each ephemeris.

1. Introduction

NY Boo and V508 Cyg are eclipsing binaries of the W UMa type (EW), many of which are characterized by a high amplitude in their light curves and continuous changes of the light curve. Since the outer atmospheres of the two stars are in contact, in many cases orbital periods are less than 1 day. In addition, mass transfer between the two components and/or angular momentum loss can cause long-term changes in the orbital period. Both systems currently lack detailed studies of their light curves and orbital parameters. The measurements and analyses performed herein help close the knowledge gap for these poorly studied systems. Both stars, with maximal visual magnitudes of 11.97 for NY Boo and 12.50 for V508 Cyg, are within the light grasp of modestly sized telescopes of about 15 to 30 cm.

2. Observations

CCD photometry of the eclipsing variable stars NY Boo and V508 Cyg was performed using a 13-inch Newtonian telescope (f/4) connected to a Moravian g2-1603 CCD camera cooled at –15° C. The FOV was 35×25 arcmin^2 and the plate scale is 1.46×1.46 arcsec^2/pixel. To perform wideband photometry the Deep-Sky GWB and BWB filter set from the company Astronomik (Astronomik 2020) was used. The obtained images were corrected by twilight flats, bias, and darks using the software AstroArt 6 (MSB Software 1998–2022).

Measurements using these filters were transformed to Johnson B and V values, and were then uploaded to the AAVSO International Database, where they fit well with data from other observers.

Figure 1 shows the transmission curves of the wide-band filters used, compared to those of standard Johnson filters.

The observations were made on six nights between 24 August and 12 September 2020 for NY Boo, and on seven nights between 24 October and 18 November 2020 for V508 Cyg. The exposure time for every frame was 120 s; a filter change (BWB, GWB, BWB, …) was performed between each recording throughout each imaging session. Using the Julian Date, the astrometric coordinates, and the geographical coordinates of the observatory, the Heliocentric Julian Date (HJD) for center of exposures was calculated.

The photometric evaluations were performed with the help of self-written programs (jupyter notebooks) based on Photutils (Bradley 2020), a module package of Astropy (Astropy Collab. *et al.* 2013). To get the instrumental magnitudes an aperture radius of five pixels was chosen, which is about one-and-a-half to double the size of the full width half maximum (FWHM) of the stars. The transformation to Johnson V and B bandpass standards was achieved using measured coefficients of first-order calculated from the standard star field M67.

Subsequently, with the help of the American Association of Variable Star Observers (AAVSO) Photometric All-Sky Survey (APASS; Henden *et al*. 2009) suitable reference stars with constant brightness and where possible nearly the same color as the variable stars were selected. With these differential photometric analysis was performed. The coordinates and magnitudes of the comparison stars used were given by the APASS catalogue and are summarized in Table 1. In Table 1, the Name field gives the names of the variables and identifications for the comparison stars. The number following the first part of the comparison star name (e.g. C0, C1) is the record number from APASS.

Figure 2 shows the field of NY Boo (in center) and the selected reference stars C0, C1, and C2 as well as the check star (CS = C3). The field of V508 Cyg with selected reference stars is shown in Figure 3.

Dense star fields like that around V508 Cyg are usually best handled by point spread function (PSF) photometry, however, there are very few programs accessible to amateurs which feature this ability. Since care was taken to ensure that no other stars lie in the measurement aperture (5 pixels), in our case the aperture method was sufficient.

After choosing suitable comparison stars their relative fluxes were determined via Equation 1:

$$\varphi_{i,rel} = \frac{\varphi_i}{\frac{1}{K-1}\sum_{k \neq i}^{K} \varphi_k} \quad (1)$$

Table 1. Variable stars and selected comparison stars for NY Boo and V508 Cyg with data from APASS (Henden *et al.* 2009).

Stat	*R.A. (2000) (°)*	*Dec. (2000) (°)*	*B*	*e_B*	*V*	*e_V*	*B – V*	*e_B – V*
NY Boo	225.2900	48.8044	12.773	0.244	12.128	0.229	0.640	0.330
	225.4580	48.8040	13.206	0.028	12.484	0.019	0.723	0.034
	225.0118	48.8985	12.888	0.008	12.154	0.041	0.734	0.042
	225.0295	48.8232	12.934	0.025	12.202	0.039	0.733	0.046
	225.2930	48.8976	13.141	0.017	12.334	0.026	0.806	0.032
V508 Cyg	308.5249	46.8711	14.034	0.245	12.918	0.435	1.116	0.499
	308.5002	46.8247	12.401	0.103	11.745	0.053	0.656	0.116
	308.3520	46.8023	12.261	0.109	11.603	0.057	0.658	0.123
	308.3519	46.9300	12.512	0.132	11.797	0.045	0.715	0.140

Table 2. Time of minima (ToM - 2.459e6) and calculated periods P.

Star	*Filter*	*ToM-1*	*σ*	*ToM-2*	σ	*ToM-3*	*σ*	*P/d*
NY Boo	V	86.4135	5.E–04	97.3615	4.E–04	105.3685	5.E–04	0.32678 ± 2e–5
	B	86.4159	8.E–04	97.3607	9.E–04	105.3682	8.E–04	
V508 Cyg	V	147.3183	4.E–04	159.4043	6.E–04	172.2676	5.E–04	0.77967 ± 1e–5
	B	147.3200	8.E–04	159.4032	8.E–04	172.2685	6.E–04	

Table 3. NY Boo ToM, Error, Type of Minima as well as Cycle Number and O – C which are calculated using the following light elements: t_n = 2459105.1980, P_n = 0.3267912.

Min. HJD	*HJD err*	*Typ*	*Epoch*	*O – C*	*Reference*
2456021.9009	0.0014	I	–9435.0	–0.02191	Diethelm (2012)
2456065.3823	0.0016	I	–9302.0	–0.00374	Hubscher and Lehmann (2013)
2456737.6407	0.0002	I	–7245.0	0.04512	Hoňková *et al.* (2015)
2456742.5429	0.0025	I	–7230.0	0.04545	Hubscher and Lehmann (2015)
2456746.3993	0.0004	I	–7218.0	–0.01965	Juryšek *et al.* (2017)
2457561.4174	0.0006	I	–4724.0	–0.01885	Juryšek *et al.* (2017)
2457879.5185	0.0007	II	–3750.5	–0.04901	Pagel (2018)
2459062.3895	0.0003	I	–131.0	0.00116	Samolyk (2020)
2459086.4153	0.0006	II	–57.5	0.00781	this paper
2459097.3615	0.0006	I	–24.0	0.00650	this paper
2459105.3685	0.0005	II	0.5	0.00712	this paper

Table 4. Fit parameters for NY Boo with one-σ uncertainties.

Linear fit parameters / NY Boo	
a_0	$-(0.0 \pm 1.4) \times 10^{-2}$
a_1	$+(0.0 \pm 2.4) \times 10^{-6}$

where φ represents the counts in ADU, i is the index of the selected star, and K is the total number of comparison stars. The results normalized relative to 1 are depicted in Figure 4 for NY Boo and in Figure 5 for V508 Cyg. As necessary a constant offset has been added to individual comparison stars to help visually differentiate the curves.

As can be seen, the flux of all comparison stars remained constant for the duration of the imaging sessions. The outliers below n = 20 and above n = 200 in Figure 4 result from the influence of high cirrus clouds passing through. These as well as the corresponding measurements for NY Boo were eliminated from consideration if deviations above 3σ (standard deviation) occurred. Hereafter, we chose C3 to be the check star (CS). Figure 5 for V508 Cyg shows a constant output in brightness for the selected comparison stars. Again, all measurements above 3σ were rejected for further calculations.

For later discussions, the following plots (Figures 6 and 7) also show the air mass of the measurements. Values above air mass 2.0 were also used but since the target and comparison stars had similar colors (B–V) they were not expected to suffer severely from differential refraction and/or color extinction.

Since the bandpass filters are changed alternately after each recording, a Savitzky-Golay (Savitzky and Golay 1964) filter was applied to interpolate (dotted curves in Figure 8), and thus generated simultaneous values for BWB and GWB for the B,V transformations. The Savitzky-Golay filter is an optimized low-pass filter for data smoothing removing high frequency noise, preserving the shape of a curve.

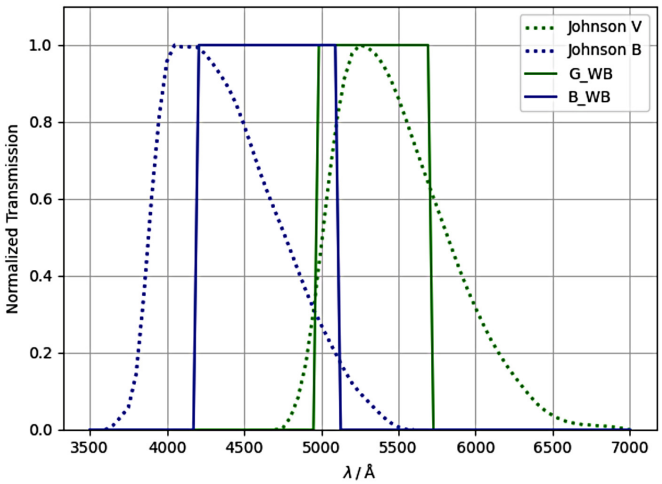

Figure 1. Normalized transmission curves of the used wide-band filters (G_{WB}, B_{WB}) and the corresponding Johnson filters.

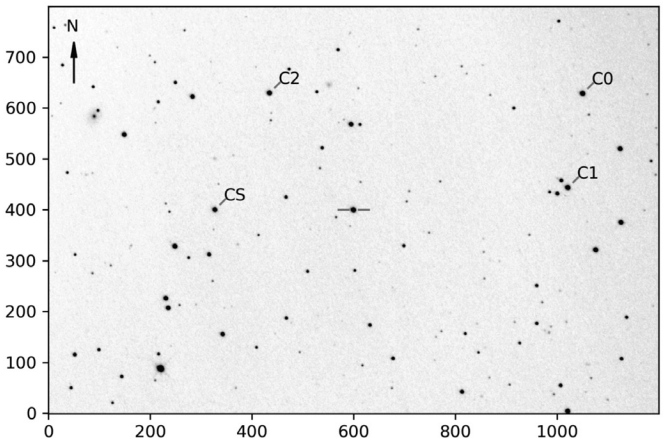

Figure 2. NY Boo with check (CS) and comparison stars (C0 to C2). The image field-of-view is 30 × 20 arcmin².

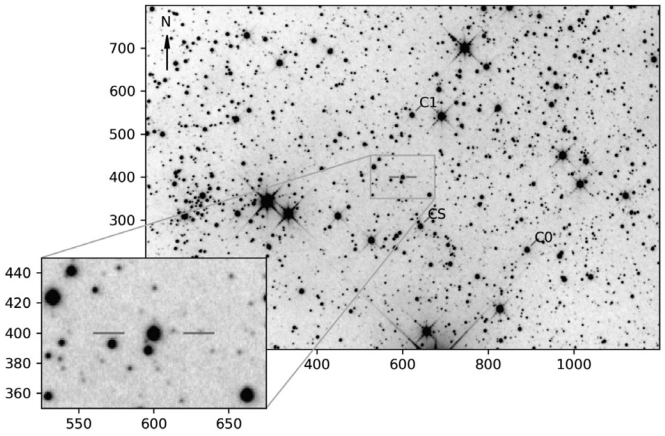

Figure 3. The image field for V508 Cyg with check (CS) and comparison stars (C0 and C2). In addition, the star-rich area around V508 has been enlarged. The FOV of the non-enlargement is 30 × 20 arcmin²; scale of inset: 3.7 × 2.5 arcmin².

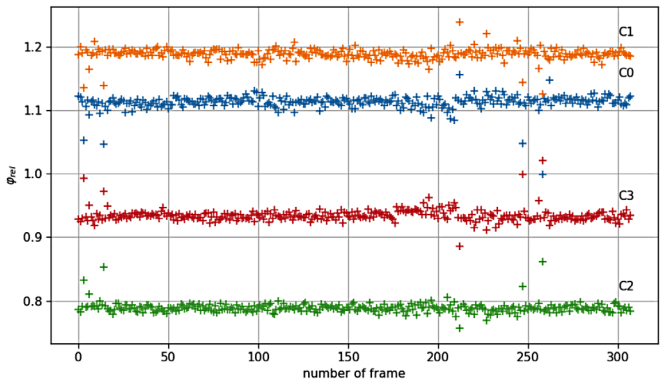

Figure 4. Relative flux for each comparison star used with NY Boo (filter = G_{WB}).

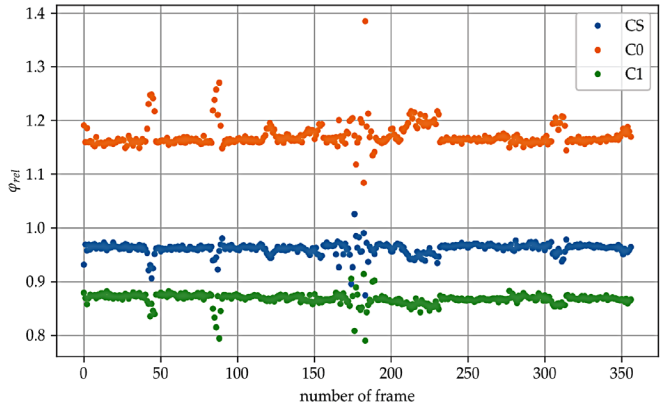

Figure 5. Relative flux for each comparison star used for V508 Cyg (filter = G_{WB}).

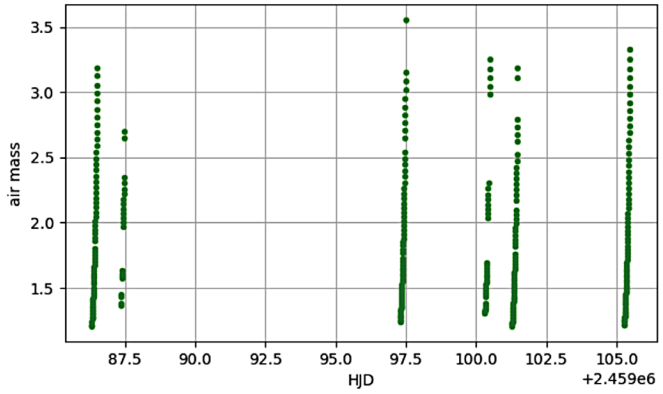

Figure 6. Air mass vs. HJD for NY Boo.

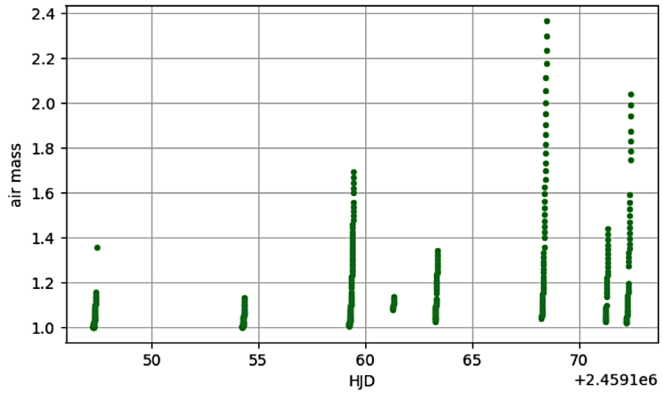

Figure 7. Air mass vs. HJD for V508 Cyg.

3. Times-of-Minima (ToM), Observed-minus-Calculated (O–C), and phase diagrams

3.1. ToM and O–C analysis

To determine the orbital period of the binaries, the times-of-minima (ToM) were calculated using all available data showing a minimum. To calculate each ToM value a slightly modified Kwee and Van Woerden method (Corp 2018) was used, whereby the light curve measurements around each minimum were smoothed with a Savitzky-Golay (SG) filter. The resulting curves were then mirrored at a point in time so that the descending and ascending branches lie above each other. To achieve this, a least square fit according to Equation 2 was performed:

$$\mathrm{Min}(t) = \left[\tfrac{1}{N}\,\Sigma_k\,(V(t - k\Delta t) - V(t + k\Delta t))\right]^{\frac{1}{2}} \qquad (2)$$

A typical result is given in Figure 9 for NY Boo.

Since no model is available at this time, the uncertainty of the ToM is determined by errors of the individual measurements and the symmetry of the curve. Figure 10 shows the curves mirrored at ToM and overlaid. The curve symmetry also determines the evaluation range for the determination of the minimum. As long as the deviations between both branches are smaller than the statistical error of the individual measurements of magnitudes, the curve is used for evaluation. In order to determine the uncertainty, the measurement points were varied within the limits of their uncertainty by means of Monte Carlo simulation and then the curve was evaluated. The scatter of the values obtained in this way was taken as the uncertainty of ToM. Because the timing is very accurate (about 1 to 2 s), its influence was neglected. With this method uncertainties in the range of 20 to 40 s (0.0002 to 0.0005 d) are obtained, depending on the course of the curves.
The same is depicted in Figures 11 and 12 for V508 Cyg.

Table 2 shows the results for both binaries. The periods P are determined using the following equations:

$$n = \mathrm{round}\left(\frac{ToM_2 - ToM_1}{P_{VSX}}\right) \qquad (3)$$

$$P = \left(\frac{ToM_2 - ToM_1}{n}\right) \qquad (4)$$

Thereby a first estimation based on the VSX data (Watson *et al.* 2014) was used (Equation 3). Afterwards Equation 4 yields the new value for the period. In addition the O–C values are calculated.

These updated orbital periods show small deviations from the original values reported by VSX for NY Boo (0.32679 d) and V508 Cyg (0.77966 d).

An O–C diagram is constructed by plotting observed ToM values minus those calculated from an ephemeris equation (y-axis) versus the corresponding epoch (x-axis). The resulting plot can be used to detect any change(s) in the orbital period of a binary star. In order to produce the necessary O–C diagrams, an ephemeris was updated using the ToM values for NY Boo (Table 3). With each new ephemeris, the old parameters (epoch t_0, period P_0) and under certain circumstances a third parameter c0 are used to calculate the observed minus calculated residuals. Depending on their behavior these are fitted using a linear or quadratic expression (see Equation 5). A straight-line relationship means the period has not changed over the defined epoch. Those O–C vs epoch plots best fit with a quadratic curve indicates a constant period change.

$$(O-C)_0 = \mathrm{ToM}(E) - (t_0 + P_0 \cdot E + c_0 \cdot E^2) = a_0 + a_1 \cdot E + a_2 \cdot E^2 \qquad (5)$$

To obtain new parameters (epoch t_n, period P_n, c_n), the O–C values have to fulfill the following condition (Equation 6):

$$(O-C)_0 = \mathrm{ToM}(E) - (t_n + P_n \cdot E + c_n \cdot E^2) = 0 \qquad (6)$$

After subtracting Equations 5 and 6 from each other and performing a coefficient comparison, the following new parameters are obtained:

$$\begin{aligned} t_n &= t_0 + a_0 \\ P_n &= P_0 + a_1 \\ c_n &= c_0 + a_2 \end{aligned} \qquad (7)$$

In addition, the fit provides the uncertainties of the parameters. Whether a linear or quadratic fit has to be used can be seen from the resulting preliminary O–C curve and the residuals of the fit.

By applying Equations 5 and 6 to historical and current ToM data new O–C values are achieved. In Figure 13 and Table 3 the results are depicted for NY Boo. Table 4 shows the corresponding fit parameters.

The updated ephemeris for NY Boo is:

$$\begin{aligned} &\mathrm{Min.(HJD)} = 2459105.1980 \pm 0.014 \\ &+ (0.32679122 \pm 0.0000024) \times E. \end{aligned} \qquad (8)$$

The situation is completely different with V508 Cyg. Only CCD data for the years 1992 to 2020 are used for the evaluation. Older photographic measurements do not fit very well. Due to the large scatter in data only the most recent data are used to calculate a linear ephemeris. The following plot (Figure 14) shows the data used and the linear fit.

A linear fit which can be used for the next few years yields the following ephemeris:

$$\begin{aligned} &\mathrm{Min.\ (HJD)} = 2459172.26816 \pm 0.00029 \\ &+ (0.7796603 \pm 0.0000001) \times E. \end{aligned} \qquad (9)$$

If the whole data set is considered a quadratic fit works best. All data used as well as the fit results are show in Figure 15.

The quadratic ephemeris is

$$\begin{aligned} &\mathrm{Min\,(HJD)} = 2459172.2629 \pm 0.0013 \\ &+ (0.7796610 \pm 0.0000045) \times E \\ &+ (1.63 \pm 0.29) \times 10^{-10} \times E^2 \end{aligned} \qquad (10)$$

The complete data set for V508 Cyg together with the references is given in Table 5.

Table 5. ToM, Error, Type of Minima as well as Epoch and O–C data for V508 Cyg.

Min HDJ	*HDJ err*	*Typ*	*Epoch*	*O – C*	*Reference*
2448834.7945	0.0005	I	–13259.0	0.0425	Goderya *et al.* (1995)
2448884.6923	0.0004	I	–13195.0	0.0420	Goderya *et al.* (1995)
2448887.8134	0.0006	I	–13191.0	0.0445	Goderya *et al.* (1995)
2448888.5912	0.0007	I	–13190.0	0.0426	Goderya *et al.* (1995)
2448889.7624	0.0001	II	–13188.5	0.0443	Goderya *et al.* (1995)
2448898.7279	0.0006	I	–13177.0	0.0437	Goderya *et al.* (1995)
2448916.6618	0.0004	I	–13154.0	0.0454	Goderya *et al.* (1995)
2448939.6589	0.0007	II	–13124.5	0.0425	Goderya *et al.* (1995)
2448834.7946	0.0003	I	–13259.0	0.0426	Goderya *et al.* (1995)
2448884.6924	0.0004	I	–13195.0	0.0421	Goderya *et al.* (1995)
2448887.8140	0.0001	I	–13191.0	0.0451	Goderya *et al.* (1995)
2448888.5999	0.0016	I	–13190.0	0.0513	Goderya *et al.* (1995)
2448889.7633	0.0013	II	–13188.5	0.0452	Goderya *et al.* (1995)
2448898.7281	0.0006	I	–13177.0	0.0439	Goderya *et al.* (1995)
2448916.6622	0.0005	I	–13154.0	0.0458	Goderya *et al.* (1995)
2448939.6591	0.0005	II	–13124.5	0.0427	Goderya *et al.* (1995)
2452802.4672	0.0027	I	–8170.0	0.0238	Hubscher *et al.* (2005)
2452834.4374	0.002	I	–8129.0	0.0279	Hubscher *et al.* (2005)
2452862.5056	0.0016	I	–8093.0	0.0284	Hubscher (2007)
2452864.4531	0.0011	II	–8090.5	0.0267	Hubscher *et al.* (2005)
2452867.5747	0.003	II	–8086.5	0.0297	Hubscher *et al.* (2005)
2452946.3186	0.0004	II	–7985.5	0.0279	Hubscher *et al.* (2005)
2453216.4645	0.0005	I	–7639.0	0.0215	Hubscher *et al.* (2005)
2453221.5264	0.0011	II	–7632.5	0.0156	Hubscher *et al.* (2005)
2453579.3945	0.0003	II	–7173.5	0.0196	Hubscher *et al.* (2006)
2453607.4575	0.0012	II	–7137.5	0.0148	Hubscher (2007)
2453612.5275	0.0009	I	–7131.0	0.0170	Hubscher *et al.* (2006)
2453621.4931	0.0008	II	–7119.5	0.0166	Hubscher *et al.* (2006)
2453637.4756	0.0013	I	–7099.0	0.0160	Hubscher *et al.* (2006)
2454073.3021	0.0002	I	–6540.0	0.0124	Hubscher and Walter (2007)
2455075.5525	0.0004	II	–5254.5	0.0095	Hubscher *et al.* (2010)
2455366.7537	0.0005	I	–4881.0	0.0075	Diethelm (2010)
2455817.3934	0.0001	I	–4303.0	0.0036	Hoňková *et al.* (2013)
2455838.4419	0.0003	I	–4276.0	0.0012	Hoňková *et al.* (2013)
2455838.4424	0.0002	I	–4276.0	0.0017	Hoňková *et al.* (2013)
2455838.4427	0.0006	I	–4276.0	0.0020	Hoňková *et al.* (2013)
2456169.4076	0.0004	II	–3851.5	0.0011	Hoňková *et al.* (2013)
2456169.4078	0.0002	II	–3851.5	0.0013	Hoňková *et al.* (2013)
2456169.4086	0.0004	II	–3851.5	0.0021	Hoňková *et al.* (2013)
2456461.3875	0.0006	I	–3477.0	–0.0017	Hoňková *et al.* (2015)
2456461.3897	0.0003	I	–3477.0	0.0005	Hoňková *et al.* (2015)
2456461.3902	0.0003	I	–3477.0	0.0010	Hoňková *et al.* (2015)
2456482.4406	0.0004	I	–3450.0	0.0005	Hoňková *et al.* (2015)
2456482.4406	0.0003	I	–3450.0	0.0005	Hoňková *et al.* (2015)
2456482.4407	0.0002	I	–3450.0	0.0006	Hoňková *et al.* (2015)
2456491.4064	0.0002	II	–3438.5	0.0002	Hoňková *et al.* (2015)
2456491.4070	0.0002	II	–3438.5	0.0008	Hoňková *et al.* (2015)
2456491.4072	0.0005	II	–3438.5	0.0010	Hoňková *et al.* (2015)
2456496.4725	0.0004	I	–3432.0	–0.0015	Hoňková *et al.* (2015)
2456496.4729	0.0002	I	–3432.0	–0.0011	Hoňková *et al.* (2015)
2456496.4734	0.0002	I	–3432.0	–0.0006	Hoňková *et al.* (2015)
2456500.3727	0.0004	I	–3427.0	0.0004	Hoňková *et al.* (2015)
2456500.3728	0.0005	I	–3427.0	0.0005	Hoňková *et al.* (2015)
2456500.3731	0.0006	I	–3427.0	0.0008	Hoňková *et al.* (2015)
2456501.5411	0.0003	II	–3425.5	–0.0006	Hoňková *et al.* (2015)
2456501.5415	0.0003	II	–3425.5	–0.0002	Hoňková *et al.* (2015)
2456501.5419	0.0003	II	–3425.5	0.0002	Hoňková *et al.* (2015)
2456542.4734	0.0002	I	–3373.0	–0.0005	Hoňková *et al.* (2015)
2456542.4735	0.0004	I	–3373.0	–0.0004	Hoňková *et al.* (2015)
2456542.4739	0.0002	I	–3373.0	0.0000	Hoňková *et al.* (2015)
2456569.3717	0.0002	II	–3338.5	–0.0005	Hoňková *et al.* (2015)
2456569.3720	0.0002	II	–3338.5	–0.0002	Hoňková *et al.* (2015)
2456569.3721	0.0003	II	–3338.5	–0.0001	Hoňková *et al.* (2015)
2456878.5074	0.0002	I	–2942.0	–0.0001	Hoňková *et al.* (2015)
2456878.5076	0.0002	I	–2942.0	0.0001	Hoňková *et al.* (2015)
2456878.5078	0.0004	I	–2942.0	0.0003	Hoňková *et al.* (2015)
2459147.3183	0.0004	I	–32.0	–0.0007	this paper
2459159.4043	0.0008	II	–16.5	0.0005	this paper
2459172.2676	0.0008	I	0.0	–0.0006	this paper
2459147.3200	0.0006	I	–32.0	0.0010	this paper
2459159.4032	0.0005	II	–16.5	–0.0006	this paper
2459172.2685	0.0006	I	0.0	0.0003	this paper

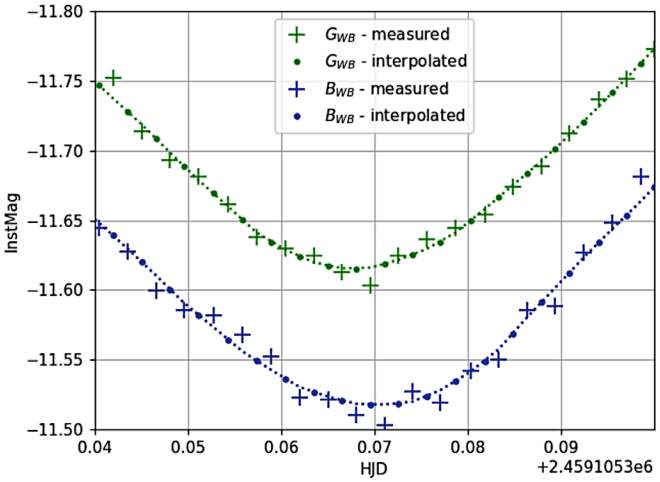

Figure 8. Example of an interpolation (dotted lines) for NY Boo (20-08-24) using a Savitzky-Golay filter (Savitzky and Golay 1964) to obtain simultaneous pairs of B_{WB}, G_{WB} data (instrumental magnitudes) for B, V transformations. Values for the B_{WB} bandpass are shifted by –0.20 mag to simplify comparison with the G_{WB} curve.

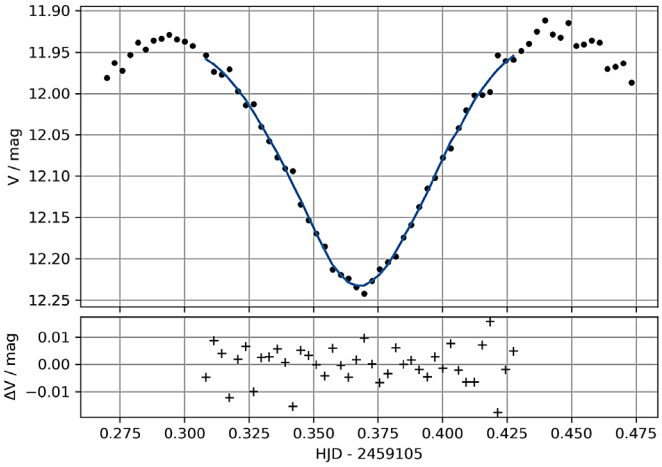

Figure 9. Upper: V-band measurements (•) of NY Boo and smoothed curve with SG filter (-); lower: the difference between both (+).

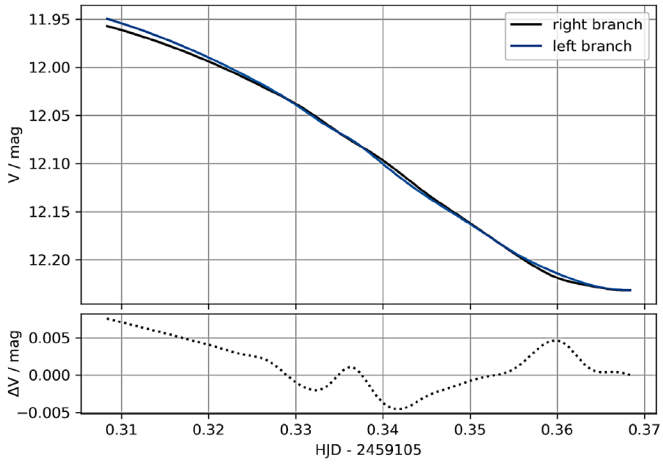

Figure 10. Upper: the interpolated right V branch of NY Boo corresponding to Figure 9, mirrored at t_{TOM} = 2459105.36843 ± 0.0005 to the left one; lower: the difference ΔV between both branches is plotted.

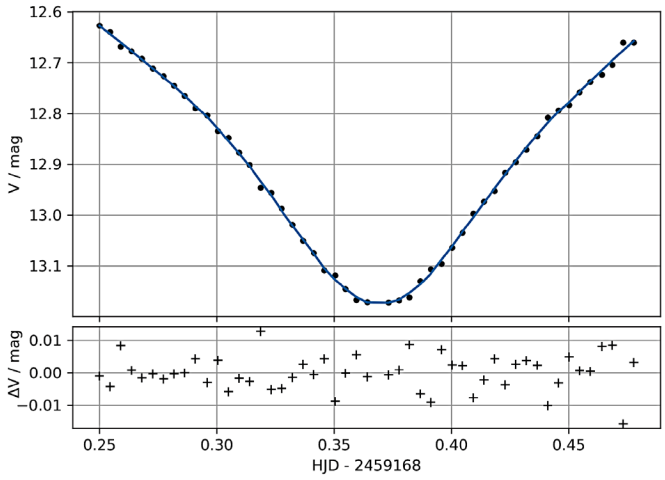

Figure 11. Upper: V band measurements (•) at V508 Cyg, smoothed curve (-); lower: the difference between both (+).

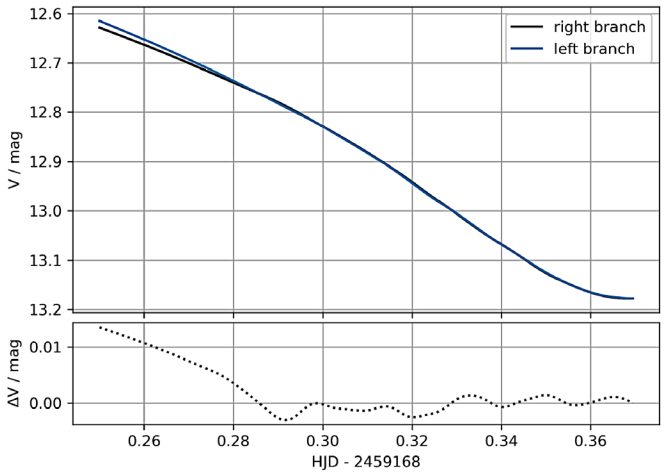

Figure 12. Upper: the right V branch of V508 Cyg (Figure 11), mirrored at tToM = 2459168.36956 ± 0.0003 to the left one; lower: the difference ΔV between the branches (Please note that in this case ΔV/mag ranges between 0.01 and some value around 0.005).

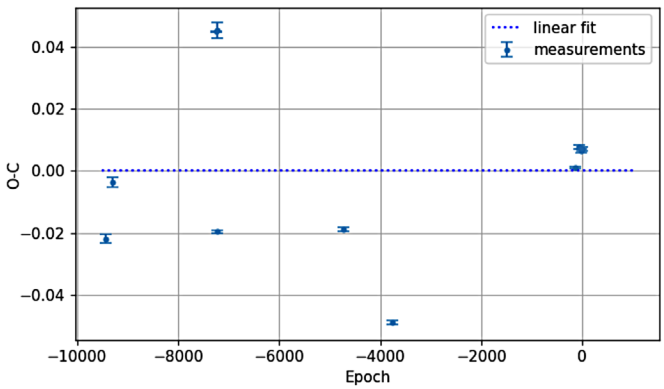

Figure 13. The best linear fit of the O–C data from NY Boo producing an intercept and a slope of 0.

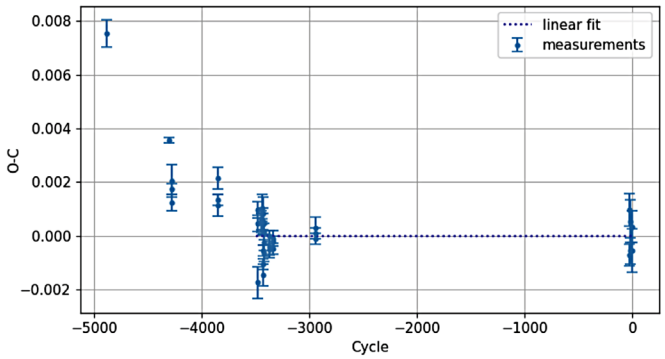

Figure 14. V508 Cyg O–C residuals for linear fit.

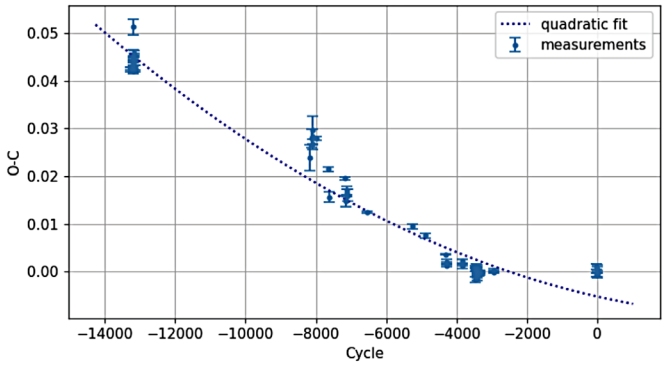

Figure 15. O–C data for V508 Cyg together with the quadratic fit curve ($a2 = (1.63 \pm 0.29) \times 10^{-10}$).

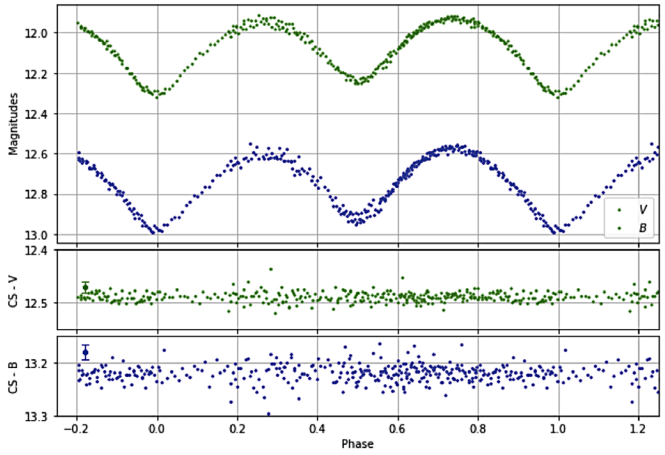

Figure 16. Phase diagram of period-folded (P = 0.326779) light curves for NY Boo in V and B. In addition the measurements of the check star (CS) are depicted below. The error bar, representing the standard deviation, is given within the subplots.

3. 2. Phase-analysis

With the help of the ToM values and the periods P obtained with Equation 4 the phase diagrams were calculated using the following equation:

$$\text{Phase} = \frac{\text{ToM}_1 - t}{P} - \text{integer}\left(\frac{\text{ToM}_1 - t}{P}\right) \qquad (11)$$

The results for NY Boo are shown in Figure 16.

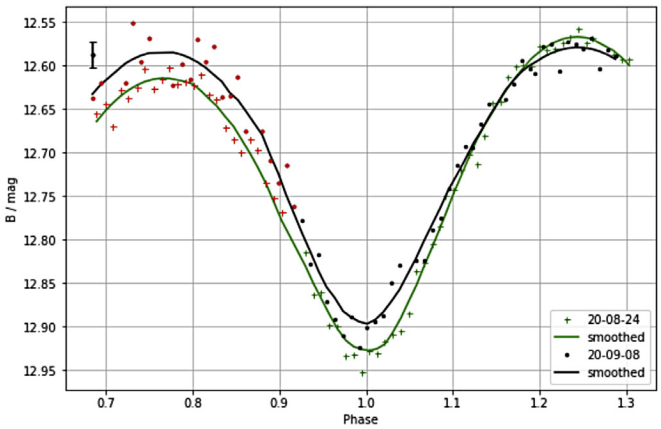

Figure 17. Phase diagram of two measurements series showing a systematic difference in B for NY Boo. The red symbols indicate air mass values larger than 2.

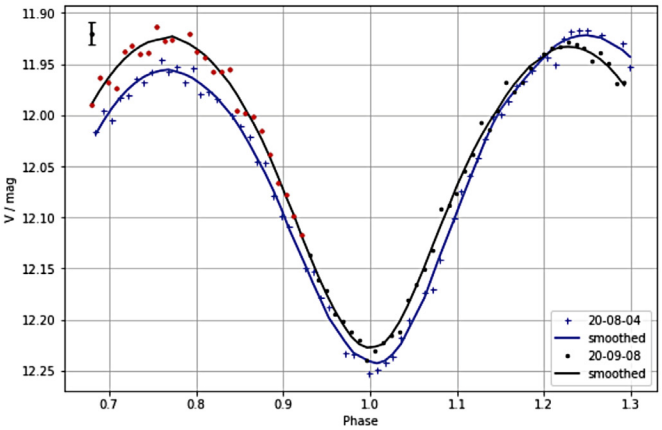

Figure 18. Phase diagram from two different dates showing a systematic difference in V for NY Boo. The red symbols indicate air mass values larger than 2.

The light curves show variations between 12.57 and 12.93 in B and between 11.93 and 12.25 in V, respectively. The difference between both filters remained constant throughout the light curves, suggesting that there is very little difference in effective temperature (T_{eff}). The color index B–V of NY Boo has a value of 0.66 ± 0.03. A primary minimum can clearly be seen (Phase = 0 and Phase = 1).

The standard deviations for the check star are in the range of 0.008 for the V filter and 0.012 for the B filter, respectively. The period-folded curves produced from data acquired between August 24, 2020, and September 12, 2020, exhibit much more scatter than would be expected. This may indicate that some event on NY Boo changed the light curve between these two relatively close dates. To investigate this further, two selected curves measured at different times (August 24, 2020, and September 8, 2020) were plotted with different symbols (Figures 17 and 18). In addition, the curves were smoothed with an SG filter. The curves clearly show a slight change of about 0.05 mag in both B and V.

On closer inspection it is noticeable that the maxima are not at the same height. The maximum difference in Figure 18 is about 0.05 mag on August 24, 2020.

To investigate whether the differences in the light curve from both dates are due to atmospheric or zeropoint effects, the behavior of the check star was analyzed in detail (see Figure 19). The difference between the mean values of the considered measurement periods are below 0.002. The standard deviations of the check star measurement at both periods are smaller than 0.01. No jumps or drift is noticeable. Considering also that the color difference between variable star and check star is only about 0.1—there should be minimal extinction effects—it can be assumed that the curves are related to varying stellar properties such as sun spots or an inhomogeneous rotating gas envelope.

To analyze color changes during darkening, the color index B-V was plotted versus phase in Figure 20. The plotted uncertainties result from the fluctuations within the two regions ($\varphi = 0$ to 0.5 and $\varphi = 0.5$ to 1). Due to the uncertainties, only small changes of $\Delta(B–V) = 0.04 \pm 0.02$ in the range 0 to 0.5 can be detected.

Figure 21 shows the same brightness investigations that were performed for the check star of V508 Cyg, which was also found to be very constant.

The phase diagram for V508 Cyg shown in Figure 22 was calculated in the same way as that for NY Boo. In contrast to NY Boo it shows no light curve anomalies. Here the maxima and minima are the same, making it impossible to visually determine which one is the primary minimum. Nonetheless, based on the linear ephemeris (Equation 8) the primary minimum (Min I) was predicted to occur on 2459147.3183, 24590147.3200, 2459172.2676, and 2459172.2685.

The light curve shows variations between 13.85 and 14.55 in B and between 12.50 and 13.18 in V, respectively. The color index B–V of this binary has a value of about 1.37 ± 0.05 (mean value during the measurement periods) and shows no variations within the uncertainties (see Figure 23).

4. Stellar properties

To accurately determine stellar temperatures, it is essential to take into account the influence of gas and dust in the galactic disk. Assuming a distance for NY Boo of D = (391) pc given in Bailer-Jones Gaia DR2 (Bailer-Jones 2015; Eur. Space Agency 2018), the interstellar extinction AV can be calculated using models A of Amôres and Lépine (2005) and A2 (Amôres and Lépine 2007). The latter takes into account the spiral structure of our galaxy. The resulting values are $A1_V = 0.10$ for the A model and $A2_V = 0.10$ for A2, respectively. In this case both models yield the same value. This allows the calculation of the color shift, i.e. reddening, using Equation 12 given in Amôres and Lépine (2005):

$$E(B-V) = \frac{A_V}{3.1} \qquad (12)$$

To obtain the intrinsic color Equation 13 was applied:

$$(B-V)_0 = (B-V) - E(B-V) \qquad (13)$$

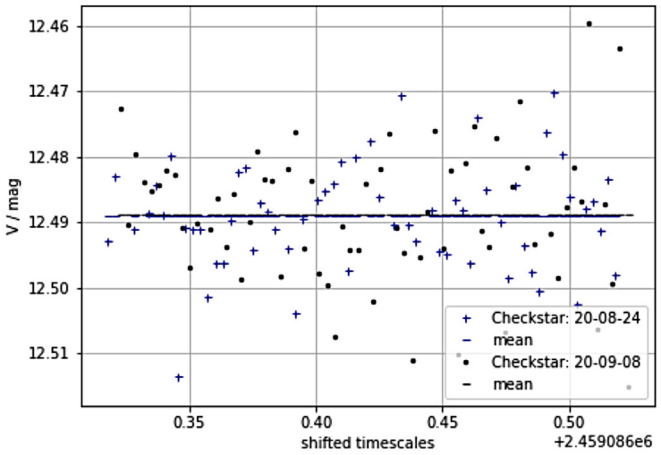

Figure 19. Brightness measurements of the check star for NY Boo on two different observation nights.

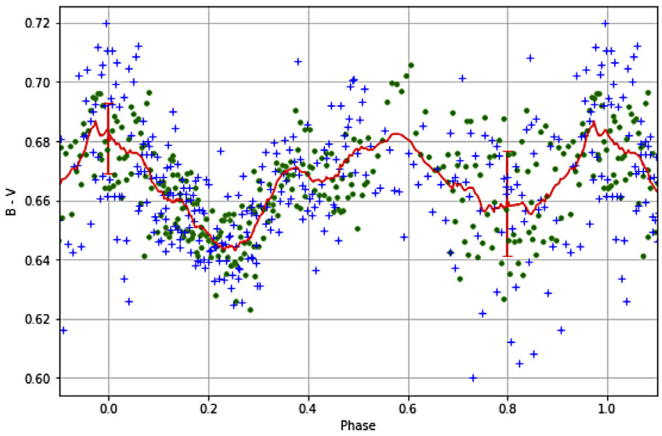

Figure 20. Moving average of (B–V) (red line) as well as B–V (blue +) and B–V (green •) of NY Boo.

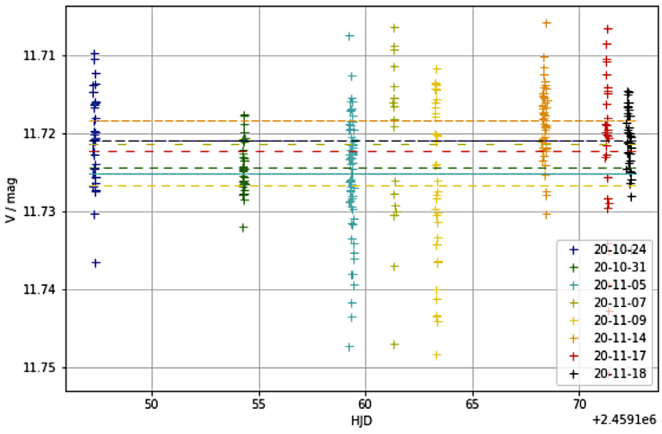

Figure 21. Brightness measurements of the check star for V508 Cyg for all observation nights.

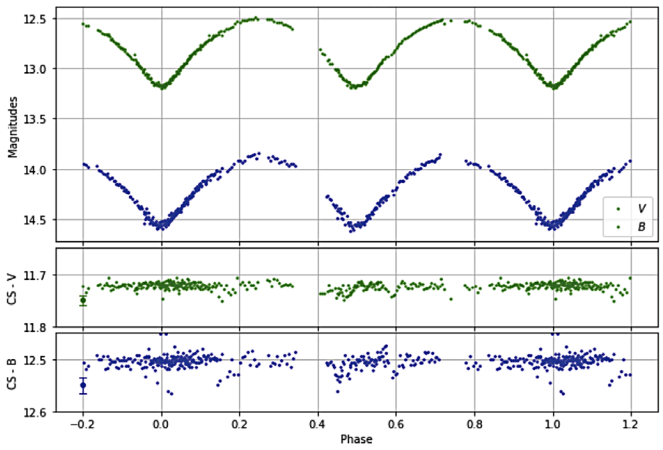

Figure 22. Phase diagram of period-folded light curves for V508 Cyg in V and B.

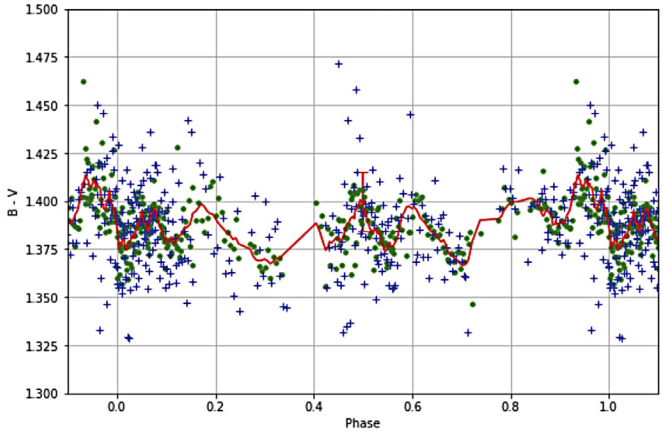

Figure 23. Moving average of (B–V) (red line) as well as B–V (blue +) and B–V (green •) for V508 Cyg.

To calculate the effective temperatures T_{eff} and the bolometric correction (BC) the polynomial approaches given by Flower (1996) and Torres (2010) were used. With the help of the distance modulus (Equation 14) and the bolometric correction (Equation 15) the values given in Table 5 were calculated.

$$M_v = V - A_V + 5 - 5\log\left(\frac{D}{pc}\right) \quad (14)$$

$$M_{bol} = M_V + BC \quad (15)$$

Besides the above equation for the determination of M_V via the distance modulus, there is, according to Rucinski and Duerbeck (1997), the possibility to determine the absolute magnitude of overcontact binary stars on the basis of their orbital period.

$$M_V(P) = -4.44\log(P) + 3.02\,(B-V)_0 + 0.12 \quad (16)$$

Equation 16 is valid for periods P = 0.2 to about 1.0 d. Our results calculated using this equation are denoted "This study" in Tables 6 and 7.

Table 6. A comparison of values for NY Boo reported in Gaia DR2 and those determined with our data for T_{eff}, BC, M_V, M_{bol}, L, and R.

	Gaia DR2	σ	*This Study*	σ
D/pc	391.8	–3.7/+3.8	346	7
A_V	—	—	0.098	0.001
(B–V)	—	—	0.66	0.01
$(B-V)_0$	—	—	0.63	0.01
T_{eff}/(K)	5668	–225/+162	5791	48
M_V	—	—	4.17	0.04
BC	—	—	–0.077	0.001
M_{bol}	—	—	4.01	0.09
$L/L_\odot$	1.76	0.03	1.54	0.06
$R/R_\odot$	1.37	–0.07/+0.12	1.23	0.03

Table 7. A comparison of values for V508 Cyg reported in Gaia DR2 and those determined with our data for T_{eff}, BC, M_V, M_{bol}, L, and R.

		Gaia DR2	σ	*This Study*	σ
D/pc		2892	–186/+212	447	53
$A1_V$		—	—	0.25	0.001
$A2_V$		—	—	1.49	0.28
(B–V)		—	—	1.37	0.05
$(B-V)_0$	$A1_V$	—	—	1.27	0.01
$(B-V)_0$	$A2_V$	—	—	0.89	0.10
T_{eff}/(K)		4597	–159/+421		
	$A1_V$			4333	83
	$A2_V$			5079	227
M_V	$A1_V$	—	—	4.49	0.15
	$A2_V$	—	—	3.28	0.31
BC	$A1_V$	—	—	–0.74	0.05
	$A2_V$	—	—	–0.27	0.09
M_{bol}	$A1_V$	—	—	5.23	0.16
	$A2_V$	—	—	3.56	0.32
$L/L_\odot$		102.3	–13.3/+13.3		
	$A1_V$	—	—	0.63	0.09
	$A2_V$	—	—	2.92	0.85
$R/R_\odot$	$A1_V$	15.95	–2.57/+1.16	1.40	0.11
	$A2_V$			2.21	0.38

To calculate the luminosity L and the radius R of one star of the investigated binaries with respect to our sun the following relations were used:

$$\frac{L}{L_\odot} = \frac{1}{2}\,10^{-0.4(M_{bol}-4.72)} \quad (17)$$

$$\frac{R}{R_\odot} = \left(\frac{1}{2}\,\frac{T_{eff,\odot}^4}{T_{eff}^4}\,10^{-0.4(M_{bol}-4.72)}\right)^{\frac{1}{2}} \quad (18)$$

In the following tables the results are given for both binaries, NY Boo (Table 6) and V508 Cyg (Table 7), respectively. The uncertainties of dependent variables were calculated using the appropriate rules for error propagation.

The same equations were applied to obtain the values for V508 Cyg. However, the position of V508 Cyg within a large nebulous region of Cygnus created a significant challenge to obtaining a realistic value for reddening, the intrinsic color $(B–V)_0$, and ultimately the effective temperature, size, and luminosity.

Looking at the results obtained from Gaia DR2, which are not adjusted for interstellar extinction, it should be fairly obvious that something is amiss with the reported distance to V508 Cyg. The calculated size (~16 $R_\odot$) and luminosity (~102 $L_\odot$) could only come from a giant star, a highly unlikely candidate for an overcontact binary with an orbital period less than 1 day.

Given the dusty region where V508 Cyg resides, results from the empirical relationship (Equation 16) described by Rucinski and Duerbeck (1997) may be biased due to significant extinction that is likely to be experienced with B and, to a lesser extent, V. Gettel *et al.* (2006) report an empirical relationship for distance (pc) where:

$$\log D = 0.2\ V_{max} - 0.18 \log (P) - 1.60\ (J - H) + 0.56. \quad (19)$$

At longer wavelengths (J and H), reduced extinction is expected. In this case the calculated distance is 447 ± 53 pc. This is nearly 6.5-fold shorter distance than that reported in Gaia DR2. This results in far less interstellar extinction with Model A (A_V = .250) but similar to the value obtained with Model A2 (A_V = 1.45), which accounts for the spiral structure of our galaxy. Whether we accept the distance results from applying Equations 14–16 or Equation 19, it is very obvious that V508 Cyg is much closer (6- to 8-fold) than that reported by Gaia DR2. Therefore the range in values reported for T_{eff}, A_V, M_V, M_{bol}, R, and L suffers from much greater variability than is suggested by the formal errors reported in Table 7. A high resolution uv-vis classification spectrum would be very helpful in trying to obtain a better estimate for the effective temperature of V508 Cyg.

5. Discussion and conclusions

5.1. NY Boo

Over a relatively short period of time between August 24 and Sept 12, 2020, light curves from this binary exhibited unexpected changes, namely, the position of both curves appeared to shift by nearly 0.05 mag. One explanation for this would be a very active photosphere due to large sunspots and a high X-ray activity. There is significant scatter around Max I (Figure 16) which could be explained by the O'Connell effect. Hot or cold starspots could also be caused by irregular mass transport or an inhomogeneous dust and gas envelope (O'Connell 1951; Davidge and Milone 1984). The nearly constant B–V color (Figure 20) indicates that both components have nearly the same effective temperature, estimated by our data to be 5791 ± 48 K. Distance data D = 392 (–3.73 / +3.80) pc derived from Gaia DR2 (Bailer-Jones 2015) are calculated from very accurate parallax measurements, the gold standard for this determination. Using the distance modulus (Equation 14), our determinations of V_{max} (11.97 ± 0.008), M_V (4.17 ± 0.04) from Equation 16, A_V (0.1), and intrinsic color ($(B–V)_0$ = 0.628 ± 0.014) indicated that NY Boo is 346 ±7 pc away from Earth. In the case of NY Boo our estimate is 13% less than the parallax-derived value. We calculate a bolometric magnitude of 4.25 ± 0.04 mag from our results. Thus, with Equations 17 and 18, a luminosity of 1.57 ± 0.01 $L_\odot$ and a radius of 1.24 ± 0.01 $R_\odot$ were determined, respectively. According to low resolution UV-vis spectra reported in LAMOST DR5 (Zhou *et al.* 2009), NY Boo is classified as a main sequence G3 star. To model the light curves properly using the Wilson-Devinney code (Terrell and Wilson 2005; Terrell 2022) further measurements will have to be made. Of particular importance since both stars exhibit partial eclipses, radial velocity determinations obtained by spectroscopy will be necessary to arrive at dependable solution for the mass ratio.

5.2. V508 Cyg

V508 Cyg is an interesting case in which the parallax-derived distance reported in Gaia DR2 and Gaia DR3 is probably very wrong. There are at least two lines of evidence that suggest this possibility. If we assume for the moment that V508 Cyg is 2892 pc distant, then in order for the apparent V magnitude to be approximately 12.5, it must be rather large (~16 $R_\odot$, Table 7) for a cool star to be this visible. Contact binaries can, in principle, consist of two evolved stars. Perhaps the best investigated example is V1309 Sco (see Stepień 2011), in which two subgiants formed a contact system before they merged, producing a so-called red nova. However, a contact binary consisting of two giants with radii of several solar radii would have an orbital period much longer than 0.78 d. Thus in the case of V508 Cyg there are contradictory data: a large distance to the star and a low temperature require correspondingly large component radii which cannot be accommodated by a tight orbit.

Secondly, there is nearly a hundred-fold difference in M_v (~ –1.30 mag, A2V) when calculated using Equation 14 when D = 2,892 pc, compared to M_v calculated (~ 3.28) using Equation 16 from Rucinski and Duerbeck (1997). Substituting M_v = 3.28 back into Equation 14 and solving for distance results in about 351 pc, a value far closer than that reported by Gaia. However, for the sake of comparison we adopted the value (447 ± 53 pc) derived from Equation 19 (Gettel *et al.* 2006), using longer wavelength (J and H) measurements that are likely to be less affected by interstellar extinction. Since estimates for interstellar extinction depended heavily on whether Model A (Amôres and Lépine 2005) or Model A2 (Amôres and Lépine 2007) is used, the corresponding calculations for M_V, BC, M_{bol}, T_{eff}, R, and L are reported in Table 7. Given the great uncertainty in all these determinations, much more data (classification spectra, radial velocities (RV), and complete multicolor light curves) will be needed to accurately describe V508 Cyg.

The O–C diagram predicts an increase (0.0132 sec/year) in the orbital period. This constant change in the orbital period can result from mass transfer, loss of angular motion, or a combination of both phenomena. In addition, the residuals from the quadratic fit (O–C vs epoch E) suggest there may be an underlying sinusoidal change in the orbital period. This could indicate the presence of a third gravitationally bound body,

although at this time there are not enough ToM values to arrive at a defensible value for orbital period (P3) of this body.

In addition, comparisons of Max I to Max II and Min I to Min II from each bandpass also show no clear differences. Here, there is no color change (B–V), which indicates that the effective temperatures of the partners are probably very close. V508 Cyg is located near the galactic plane where strong gas and dust accumulation lead to a strong color shift at shorter wavelengths like B. A comparison with other measurements (J and H passbands) suggests an effective temperature in the range of 4333 to 5079 K.

The distance to V508 Cyg reported in Gaia DR2 (2,892 pc) is highly suspect. In order for it to be detected this far away with a relatively small aperture telescope it would have to be a highly luminous K class giant. However, the established orbital period (0.779658 d) is simply too short for two stars that are 16 solar radii in size. Estimates using Equations 16 (Rucinski and Duerbeck 1997) and 19 (Gettel *et al.* 2006) suggest that the approximate distance is between 350 and 450 pc, thereby keeping this system on the main sequence. Nonetheless, a high resolution uv-vis classification spectrum will be necessary to confirm this assignment. Under any circumstances, V508 Cyg would be a worthy candidate for further study.

6. Acknowledgements

We acknowledge with thanks the variable star observations from the AAVSO International Database contributed by observers worldwide and used in this research. We acknowledge also the BRNO database for reporting their observations. This research made use of Astropy, a community-developed core Python package for Astronomy (Astropy Collaboration *et al.* 2013) and Photutils, an Astropy package for detection and photometry of astronomical sources (Bradley *et al.* 2020). This research has made use of the VizieR catalogue access tool, CDS, Strasbourg, France (DOI: 10.26093/cds/vizier). The original description of the VizieR service was published in Ochsenbein *et al.* (2000).

We thank the referee for the thorough review and a lot of helpful comments and suggestions.

References

Amôres, E. B., and Lépine, J. R. D., 2005, *Astron. J.*, **130**, 659.
Amôres, E. B., and Lépine, J. R. D., 2007, *Astron. J.*, **133**, 1519.
Astronomik. 2020, astronomical filters (https://www.astronomik.com/de/photographic-filters/deep-sky-rgb-colour-filters.html).
Astropy Collab., Robitaille, T. P., *et al.* 2013, *Astron. Astrophys.*, **558A**, 33.
Bailer-Jones, C. A. L. 2015, *Publ. Astron. Soc. Pacific*, **127**, 994.
Bradley, L. 2020, Photutils package (https://github.com/astropy/photutils/tree/1.0.1).
Corp, L. 2018, in *Proceedings for the 37th Annual Conference of the Society for Astronomical Sciences*, ed. B. Buchheim, Science, Society for Astronomical Sciences, Rancho Cucamonga, CA, 255.
Davidge, T. J., and Milone, E. F. 1984, *Astrophys. J., Suppl. Ser.*, **55**, 571.
Diethelm, R. 2010, *Inf. Bull. Var. Stars*, No. 5945, 1.
Diethelm, R. 2012, *Inf. Bull. Var. Stars*, No. 6029, 1.
European Space Agency. 2018, Gaia Data Release 2 (https://www.cosmos.esa.int/web/gaia/dr2).
Flower, P. J. 1996, *Astrophys. J.*, **469**, 355.
Gettel, S. J., Geske, M. T., and McKay, T. A. 2006, *Astron. J.*, **131**, 621.
Goderya, S. N., Leung, K. C., ands Schmidt, E. G. 1995, *Astron. J.*, **110**, 346.
Henden, A. A., Welch, D. L., Terrell, D., and Levine, S. E. 2009, *Bull. Amer. Astron. Soc.*, **41**, 669.
Hoňková, K., *et al.* 2013, *Open Eur. J. Var. Stars*, **160**, 1.
Hoňková, K., *et al.* 2015, *Open Eur. J. Var. Stars*, **168**, 1.
Hubscher, J. 2007, *Inf. Bull. Var. Stars*, No. 5802, 1.
Hubscher, J., and Lehmann, P. 2013, *Inf. Bull. Var. Stars*, No. 6070, 1.
Hubscher, J., and Lehmann, P. B. 2015, *Inf. Bull. Var. Stars*, No. 6149, 1.
Hubscher, J., Lehmann, P. B., Monninger, G., Steinbach, H.-M., and Walter, F. 2010, *Inf. Bull. Var. Stars*, No. 5941, 1.
Hubscher, J., Paschke, A., and Walter, F. 2005, *Inf. Bull. Var. Stars*, No. 5657, 1.
Hubscher, J., Paschke, A., and Walter, F. 2006, *Inf. Bull. Var. Stars*, No. 5731, 1.
Hubscher, J., and Walter, F. 2007, *Inf. Bull. Var. Stars*, No. 5761, 1.
Juryšek, J., et. al. 2017, *Open Eur. J. Var. Stars*, **179**, 1.
O'Connell, D. J. K. 1951, *Riverview Coll. Obs. Publ.*, **2**, 85.
Ochsenbein, F., Bauer, P., and Marcout, J. 2000, *Astron. Astrophys., Suppl. Ser.*, **143**, 23.
Pagel, L. 2018, *Inf. Bull. Var. Stars*, No. 6244, 1.
Rucinski, S. M., and Duerbeck, H. W. 1997, *Publ. Astron. Soc. Pacific*, **109**, 1340.
Samolyk, G. 2020, *J. Amer. Assoc. Var. Star Obs.*, **48**, 256.
Savitzky, A., and Golay, M. J. E. 1964, *Anal. Chem.*, **36**, 1627.
Stępień, K. 2011, *Astron. Astrophys.*, **531A**, 18.
Terrell, D. 2022, *Galaxies*, **10**, 8 (DOI: 10.3390/galaxies10010008).
Terrell, D., and and Wilson, R. E. 2005, *Astrophys. Space Sci.*, **296**, 221.
Torres, G. 2010, *Astron. J.*, **140**, 1158.
Watson, C., Henden, A. A., and Price, C. A. 2014, AAVSO International Variable Star Index VSX (Watson+, 2006–2014; https://www.aavso.org/vsx).
Zhou, A.-Y., Jiang, X.-J., Zhang, Y. P., and Wei, J.-Y. 2009, *Res. Astron. Astrophys.*, **9**, 349.